Non-linear systems

KU Leuven H03D9a
Prof. Johan Suykens & Prof. Dirk Roose

Tomas Fiers
August 2018

Contents

1 Stability of equilibrium points & bifurcations

1.1 Simple population model

The population model has in general two solutions (and hence two fixed points) for $\dot{N} = 0$, namely

$$N_1 = 0 \quad \text{and} \quad N_2 = K\frac{\alpha - \beta}{\alpha}.$$

The stability of these fixed points in function of α and β can be summarised as follows:

Parameter region	Fixed points
$\alpha < \beta$	$N_1 = 0$: stable $N_2 < 0$: unstable
$\alpha = \beta$	$N_1 = N_2 = 0$: half-stable (unstable for $N < 0$, stable for $N > 0$)
$\alpha > \beta$	$N_1 = 0$: unstable $N_2 > 0$: stable

The system thus undergoes a transcritical bifurcation at $\alpha = \beta$. Note that the fixed point $N_2 < 0$ is not meaningful in this model, as N represents a non-negative population count.

For the given parameter values, $\alpha > \beta$. Using the above results, we therefore find an unstable fixed point $N_1 = 0$, and a stable fixed point $N_2 = K(\alpha - \beta)/\alpha = 4\,023\,913$. As the population starts at $N > 0$, it will evolve towards N_2. The difference between $N(t)$ and $N(\infty) = N_2$ decays exponentially, as a Taylor approximation of $\dot{N}$ around N_2 can show.

1.2 Gene control model

For $r = 0$, the system equations become decoupled:

$$\dot{x} = \frac{\alpha_1}{2} - x$$
$$\dot{y} = \frac{\alpha_2}{2} - y.$$

We can therefore analyse them separately. It is clear that there is one fixed point, at $x^* = \alpha_1/2$ and $y^* = \alpha_2/2$. It is a globally stable attractor, as $\forall x < x^*,\ \dot{x} > 0$ and $\forall x > x^*,\ \dot{x} < 0$ (and analogously for $\dot{y}$ and y^*). The fixed point is thus an attracting star.

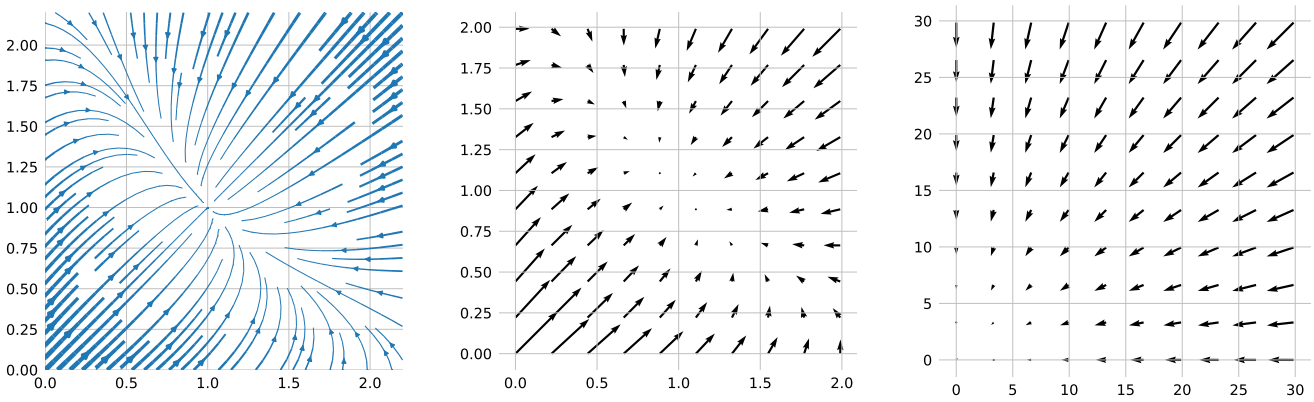

Figure 1: **There is only one fixed point for $0 \leq r \leq 2$.** Phase space plots of the gene control model, for $r = 1$ and $\alpha_1 = \alpha_2 = 2$. *Left*: some (partial) trajectories in phase space. Thicker lines represent a higher local speed. Note the attractor at $(1, 1)$. *Middle*: local velocities, evaluated on a grid. *Right*: same as middle, but for a larger region in phase space.

For $r \geq 0$ and $\alpha_1 = \alpha_2 = 2$, the equilibrium equations become

$$x(1 + y^r) = 2$$
$$y(1 + x^r) = 2.$$

It is easily verified that $(1, 1)$ is a solution and hence a fixed point. We have already shown that it is the only fixed point for $r = 0$. Plotting the gradient in phase space for different $r \in (0, 2)$ strongly suggests that it is also the only fixed point for nonzero $r < 2$ (at least for $x \geq 0$ and $y \geq 0$). See e.g. fig. 1 for $r = 1$. As a final piece of evidence, different trajectories simulated back in time all either tend towards (∞, ∞) or cross into forbidden $x < 0,\ y < 0$ territory.

To analyse the stability of the $(1, 1)$ fixed point, we approximate $(\dot{x}, \dot{y})$ as a linear system around this point. The Jacobian of $(\dot{x}, \dot{y})$ evaluated in $(1, 1)$ is:

$$\begin{pmatrix} -1 & -\frac{r}{2} \\ -\frac{r}{2} & 1 \end{pmatrix}.$$

It has two distinct eigenvalue-eigenvector pairs:

$$\lambda_1 = -\frac{r}{2} - 1, \quad \mathbf{v}_1 = (1,\ 1)$$
$$\lambda_2 = \frac{r}{2} - 1, \quad \mathbf{v}_2 = (-1,\ 1).$$

For $0 \leq r < 2$, $\lambda_1 \in (-2, -1]$ and $\lambda_2 \in [-1, 0)$. Both eigenvalues are negative, and $(1, 1)$ is therefore a stable node. Because $\lambda_1 < \lambda_2$, $\mathbf{v}_1 = (1,\ 1)$ is the fast eigendirection and $\mathbf{v}_2 = (-1,\ 1)$ is the slow eigendirection, as can be seen in fig. 1. (For $r = 0$, both eigenvalues are equal; i.e. $(1, 1)$ is then a star node).

Based on phase space plots for different values of r, it seems that a supercritical pitchfork bifurcation occurs at $r = 2$. As the problem is symmetrical for $\alpha_1 = \alpha_2$, this is expected (**Strogatz1994 Strogatz1994 Strogatz1994**).

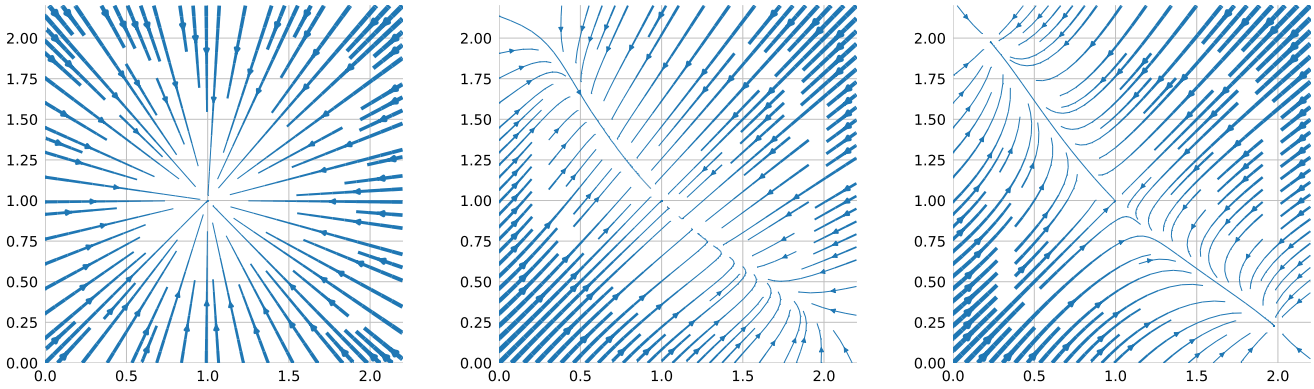

Figure 2: **Topologies of phase space**. *Left*: $r = 0$. The single fixed point is an attracting star node. (For the intermediate case between $r = 0$ and $r = 2$, see fig. 1).*Middle*: $r = 2$. There is still only one fixed point. Because we are exactly at the bifurcation point, the approach to the fixed point occurs very slowly (i.e. no longer exponentially fast). This is known as critical slowing down. *Right*: $r = 3$. There are three fixed points: a saddle point at $(1, 1)$, and two attracting nodes (mirror symmetric around $y = x$).

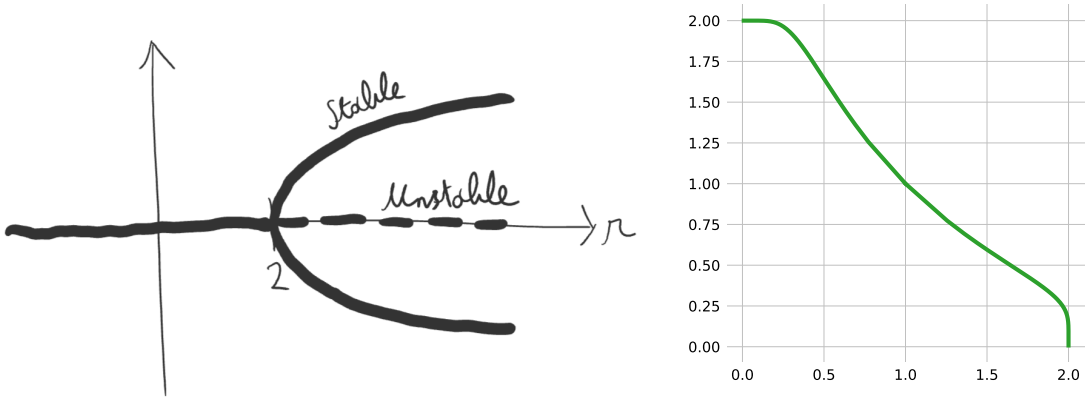

Figure 3: **The gene control model undergoes a supercritical pitchfork bifurcation**. *Left*: sketch of the bifurcation diagram. The vertical axis denotes distance in the bifurcation subspace from the $(1, 1)$ point. *Right*: the one-dimensional bifurcation subspace embedded in two-dimensional phase space.

Figure 2 shows the different types of phase portrait that occur as $r \geq 0$ is varied. Figure 3 sketches the bifurcation diagram.

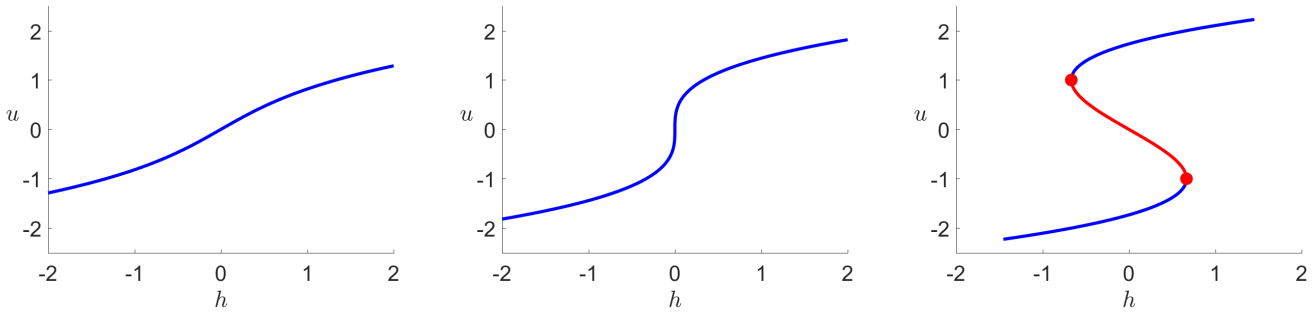

Figure 4: **(h, u)-bifurcation diagrams**. Blue lines denote stable equilibria, red lines denote unstable equilibria, and red circles indicate saddle-node bifurcations. Left: $r = -1$. (Phase space topologies for other $r < 0$ are equivalent). Center: $r = 0$. Right: $r = 1$. (Phase space topologies for other $r > 0$ are equivalent).

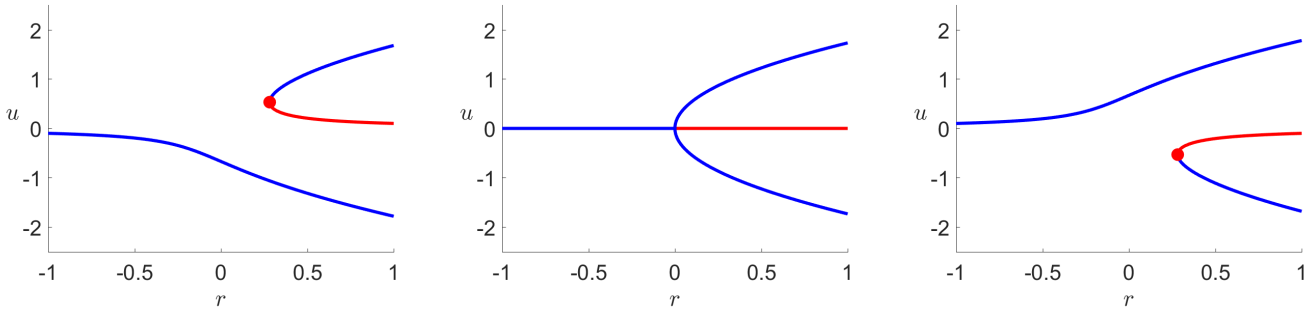

Figure 5: **(r, u)-bifurcation diagrams**. Colors as in fig. 4. Left: $h = -0.1$. Center: $h = 0$. Right: $h = 0.1$.

2 Imperfect bifurcations

When h is varied, we observe saddle-node bifurcations for $r > 0$ (see fig. 4). For $r = 0$, these two points coalesce into a single degenerate bifurcation point at $h = 0$, where u experiences critical slowing down as it approaches the origin. This is a codimension-2 bifurcation.

When r is varied, only one saddle-node bifurcation can be observed for each fixed h (fig. 5). The saddle-node appears at positive u for negative h, and vice versa. For $h = 0$, the system undergoes a supercritical pitchfork bifurcation (at $r = 0, u = 0$). h is an 'imperfection' parameter: without it, the system is symmetric (i.e. identical for $u = -u$).

Figure 6 shows the continuation curve of the saddle-node bifurcations. We note that there are indeed no saddle-node bifurcations for $r < 0$, and that there are two possible saddle-node bifurcations for $r > 0$, as already seen in figs. 4 and 5. The symmetries observed in those figures are also apparent here. The codimension-2 bifurcation is visible

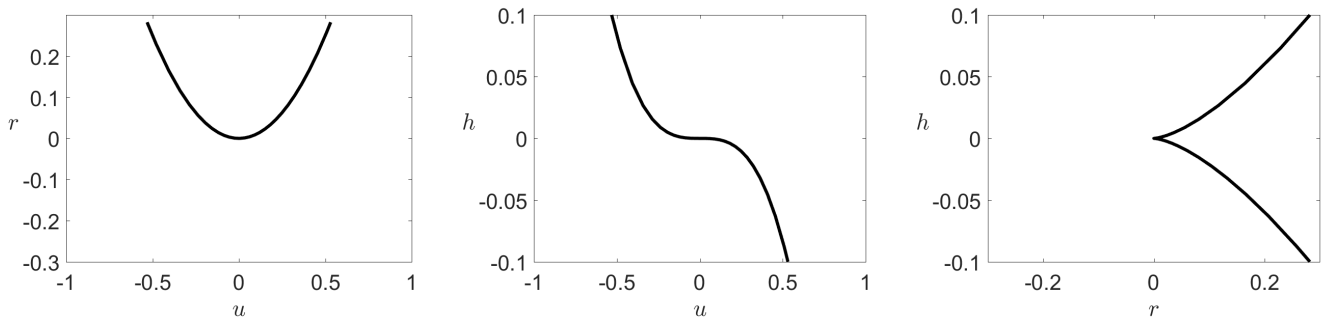

Figure 6: **Fold curve**. Continuation of the saddle-node bifurcations (the red circles in figs. 4 and 5), projected on the (u, r), (u, h), and (r, h) planes.

in the (r, h) plane as the cusp point at $(0, 0)$ (where the two branches meet tangentially). In (u, r, h)-space, the continuation curve has a spiral-like shape. It starts out in the $(+, +, -)$-octant, climbing towards the $(0, 0, 0)$ cusp point, where it is locally flat along the h-axis. It then continues its climb in the $(-, -, +)$-octant.

We now discuss some parameters of the numeric continuation algorithm used **Schilder2018**. `cont.ItMX` is the maximum number of continuation steps taken along a branch. Reducing this parameter (in conjunction with shorter step sizes) results in shorter found branch segments.

For each continuation step, a solution (i.e. a fixed point) is searched for some parameter step size Δh. The maximum number of iterations of this root-finding phase can be specified with `corr.ItMX`. If no root is found within this number of iterations, the parameter step size Δh is reduced, and the root-finding phase repeats. The maximum and minimum step sizes Δh can be set using `h_max` and `h_min`, respectively.

Choosing step sizes `h_max` that are too large can result in missed branches (fig. 7). The continuation algorithm assumes a relatively smooth branch shape. When h becomes very small however, the derivative along the branch at $(0, 0)$ becomes very steep, and this assumption is violated. Only with small step sizes can the branch still be followed. Choosing *minimum* step sizes `h_min` that are too large can also miss branches, or even report non-existent saddle-node bifurcations (fig. 8).

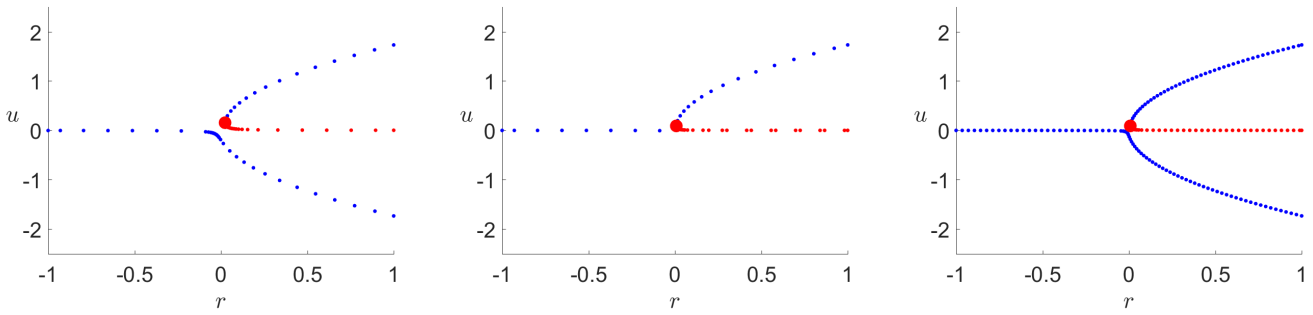

Figure 7: **Continuation is a discrete process**. Bifurcation diagrams for $h = -0.0025$ (left) and $h = -0.0005$ (center and right). Each dot is the solution of one continuation step. Colors as in fig. 4. The (maximum) step size `h_max = 0.2` is identical in the left and center figures; yet in the center figure, the lower stable branch is not found. When the step size is decreased to `h_max = 0.05` however, the lower branch is found (right). (Other parameters were left to their default COCO settings: `cont.ItMX = 100`, `corr.ItMX = 10`, `h_max = 0.01`, etc).

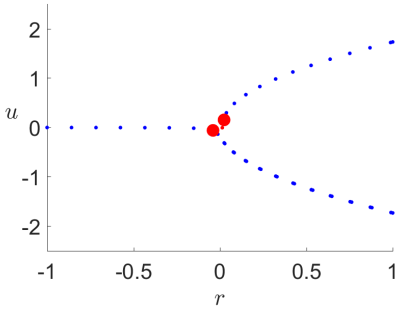

Figure 8: **Incorrect second saddle-node bifurcation**. Bifurcation diagram for $h = -0.0025$ and `h_min = h_max = 0.2`. (Other parameter settings as in fig. 7). Note the missed unstable branch, and the two saddle-node bifurcations (where there should only be one).

3 Study of a predator-prey model

We study the system

$$\dot{x} = x(x-a)(1-x) - bxy$$
$$\dot{y} = xy - cy - d,$$

with $a = 0.1$ and $b = 1.5$. The following could be an ecological interpretation of this system as a predator-prey model:

The $-d$ term represents a constant decline of species y; This would correspond to a linear decrease in y over time, with slope d, if this was the only term present. Maybe an environmental agency eliminates a fixed number d of y-type animals every time period, to keep the ecosystem balanced.

The $-cy$ term represents a proportional pressure on y, corresponding to an exponential decline of y over time with time constant $1/c$ (i.e. faster decline for larger c). There might be a fixed amount of resources available for the y species. Then, a larger number of y animals will result in a proportionally smaller amount of resources per animal, resulting in the proportional pressure on y.

The xy term represents a growth of y that is both proportional to the other species and to itself. For constant x, this would correspond to exponential growth of y with time constant $1/x$ (i.e. faster growth for more x). y could be a multiplying parasite, and x could be its host.

The $-bxy$ term represents a decline of the x species proportional to both itself and to the other species y. For constant y, this would correspond to an exponential decline of x with time constant $1/(by)$. The y parasite might be pathological for x. Both more parasites y and more hosts x yield a higher probability of transmitting the parasite between hosts.

Finally, the $x(1-x)$ factor of the first term describes logistic growth (i.e. exponential growth from the origin, which switches halfway to exponential decay up to a carrying capacity – which is 1 in this case). This is a common model for constrained species growth. The $(x-a)$ multiplier has the effect that the growth does not start until x reaches a: for $x < a$, the species will decline instead of grow. This could model the fact that more than a few individuals are necessary for succesful long-term reproduction.

In summary, the parameters (a, b, c, d) could be given the following names:

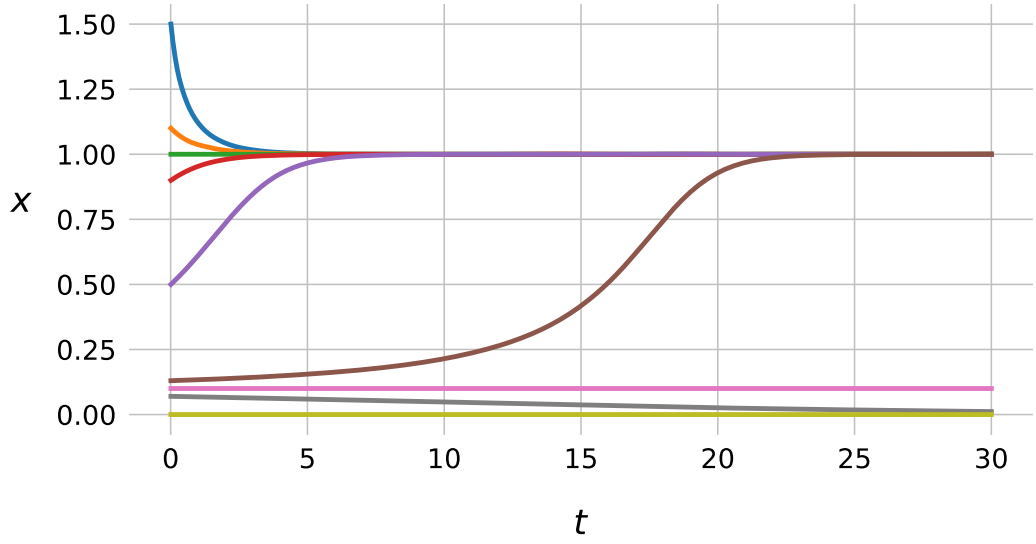

Figure 9: **Prey without predators**. Simulated trajectories $x(t)$ for $y = 0$ and different initial values x_0 (from top to bottom: 1.5, 1.1, 1.0, 0.9, 0.5, 0.13, 0.1, 0.07 and 0). Note the stable fixed points at 0 and at the carrying capacity 1, and the unstable fixed point at $a = 0.1$.

a Minimum prey population

b Predator lethality

c Predator decay rate

d External predator elimination rate

3.1 A qualitative study for $d = 0$

Simulating the system for $y = 0$ confirms the predictions made above for the standalone behaviour of $x(t)$ (fig. 9): logistic growth above the threshold a, and decay to zero below this threshold.

The system has four fixed points for $d = 0$. Three of these lie on the x-axis. They are listed in table 1, together with the eigenvalues and corresponding eigenvectors of the Jacobian in these points. The fourth fixed points has coordinates $(c,\ (c-a)(1-c)/b)$, and the eigenstructure of its Jacobian is rather more.. complex. Its trace τ and determinant Δ have simpler analytical expressions however: $\tau = c(1 + a - 2c)$ and $\Delta = c(c - a)(1 - c)$. The following paragraphs describe the topological structure near these four fixed points.

$(0,\ 0)$ is an attractor node for $c > 0$. In the common case that $c > a = 0.1$, the x-axis is the slow eigendirection. When $c < a$, the y-axis is the slow eigendirection.

$(a,\ 0)$ is a saddle when $c > a$. Its stable manifold is then the x-axis, and its unstable manifold is locally spanned by $(ab/(c - a^2),\ 1)$, which is an upwards pointing vector,

Fixed point	Eigenvalues	Eigenvectors
$(0,\ 0)$	$-a$	$(1,\ 0)$
	$-c$	$(0,\ 1)$
$(a,\ 0)$	$a - a^2$	$(1,\ 0)$
	$a - c$	$(ab/(c - a^2),\ 1)$
$(1,\ 0)$	$a - 1$	$(1,\ 0)$
	$1 - c$	$(-b/(2 - c - a),\ 1)$

Table 1: **Fixed points on the x-axis**. (x, y)-coordinates of the fixed points, and eigenvalue-eigenvector pairs of the Jacobian.

rotated slightly right. When $c < a$, both dimensions are unstable, and $(a,\ 0)$ is then a repellor node. For $c > a^2$, the slow eigendirection is $(ab/(c - a^2),\ 1)$. For $c < a^2$, the x-axis is the slow eigendirection.

$(1,\ 0)$ is a saddle when $c < 1$. With $a = 0.1$, the stable manifold is the x-axis, and the unstable manifold is locally spanned by $(-b/(2 - c - a),\ 1)$, which is an upwards pointing vector, rotated slightly *left*. When $c > 1$, both dimensions become stable, and $(1,\ 0)$ is then an attracting node. Because $c < 1.5$ in this exercise, the slow eigendirection is $(-b/(2 - c - a),\ 1)$.

The final fixed point, $(c,\ (c - a)(1 - c)/b)$, has a wider range of behaviours (fig. 10). It is a saddle for $c > 1$, and for $0 < c < a$. It is an unstable node for $a < c < c_u$, an unstable spiral for $c_u < c < (a + 1)/2$, a stable spiral for $(a + 1)/2 < c < c_s$, and a stable node for $c_s < c < 1$. c_u and c_s are the solutions to $4\Delta = \tau^2$ (**Strogatz1994 Strogatz1994 Strogatz1994**). For $a = 0.1$, c_u and c_s are numerically determined to be $c_u = 0.1259..$ and $c_s = 0.8783...$

The separatrices between basins of attraction are the stable manifolds of saddles. The stable manifold of a saddle at $(x^*,\ y^*)$ can be found numerically by simulating a trajectory back in time. The initial point of this trajectory is $(x^* + \Delta x,\ y^* + \Delta y)$, where Δx and Δy are small perturbations on the line spanned by the eigenvector of the Jacobian corresponding to this stable manifold (i.e. the eigenvector with a negative eigenvalue).

This technique is used in fig. 11 to draw the separatrices between basins of attraction. Note that the separatrices themselves are also one-dimensional 'manifolds of attraction', namely for the saddles.

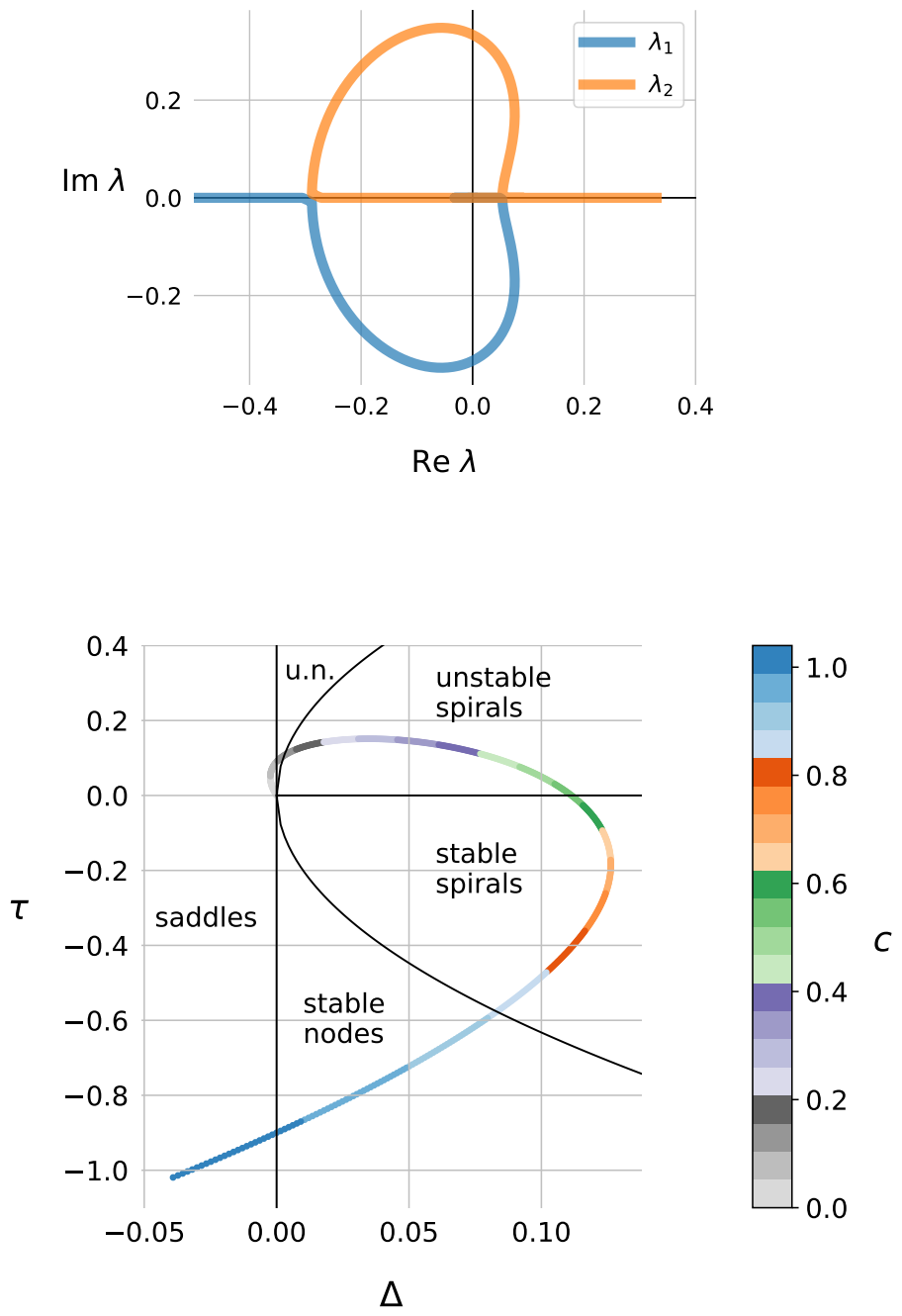

Figure 10: **Linear system analysis of the fixed point $(c,\ (a-c)(c-1)/b)$.** *Top*: eigenvalues of the Jacobian at the fixed point, for $a = 0.1$ and $c \in [0, 1.5]$ ($c = 0$ in the origin, and $c = 1.5$ at the far right for λ_2 and at the far left, outside the figure, for λ_1). *Bottom*: trace τ and determinant Δ of the Jacobian at the fixed point, for $a = 0.1$ and $c \in [0, 1.04]$ (for larger c, the (τ, Δ) curve simply extends further down in the 3rd quadrant). u.n.: unstable nodes.

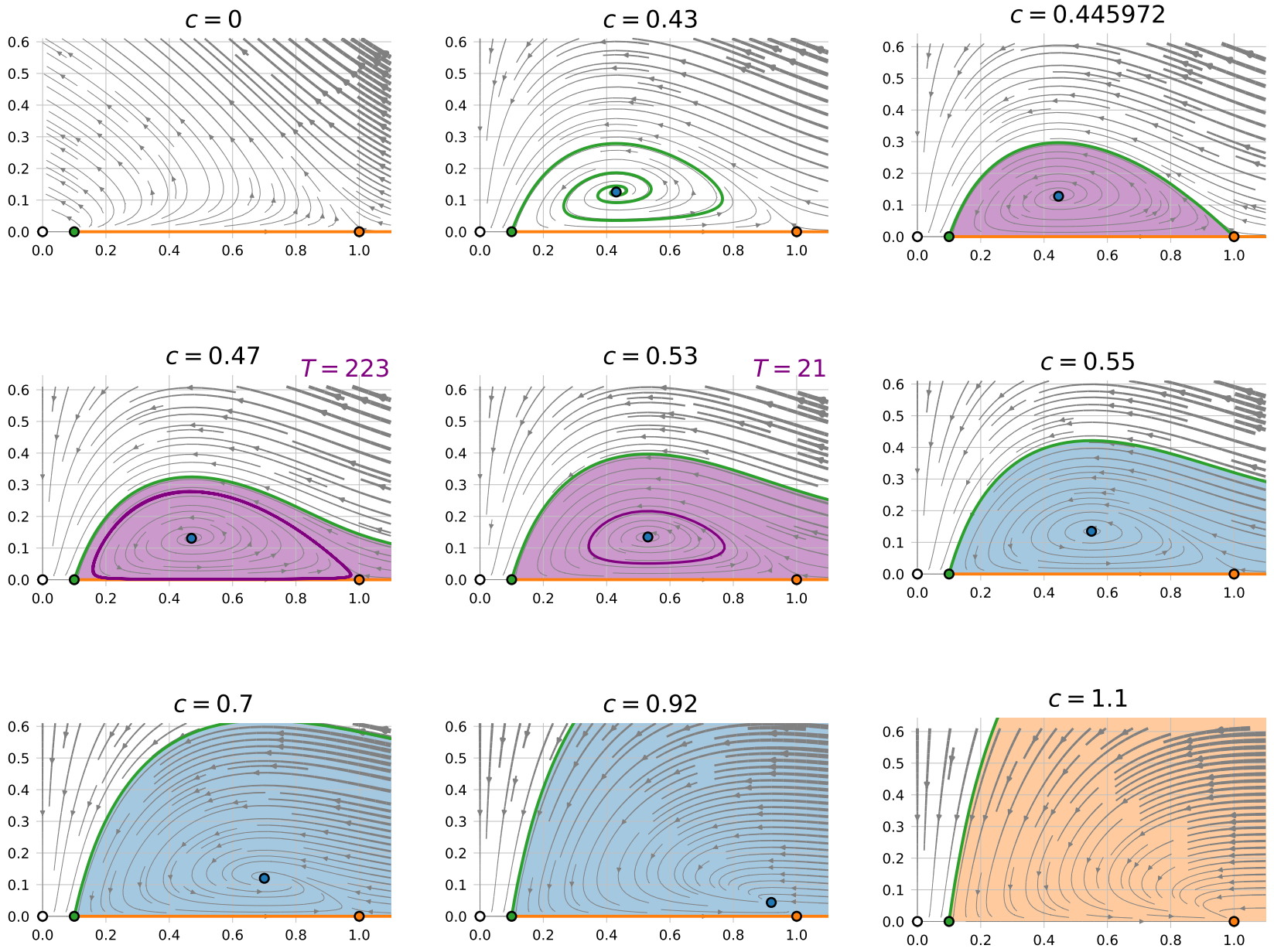

Figure 11: **Phase space diagrams for different predator decay rates c.** Colored circles represent fixed points. Their manifolds of attraction are indicated with the same color. (At $c = 0$, the entire y-axis consists of fixed points). The limit cycle for $c_h = 0.446... < c < 0.55$, its basin of attraction, and its period T are indicated in purple.

Figure 11 is consistent with the analysis made above: the origin is indeed always an attractor node for $c > 0$; the role of $(a,\ 0)$ indeed switches from repellor node to saddle (top row), just as $(1,\ 0)$ switches from saddle to attractor node (bottom row); and finally, the fixed point $(c,\ (c-a)(1-c)/b)$ takes on the subsequent roles predicted in fig. 10: from unstable spiral (top and middle row), to center (middle row, rightmost column), to stable spiral, attractor node, and saddle (bottom row).

This sequence of behaviours of the last fixed point can also be observed by following the eigenvalues λ_i of its Jacobian in the complex plane (fig. 10). For $c > 1$, the eigenvalues start out on opposite ends of the real axis, and the fixed point is indeed a saddle. When c then decreases, the eigenvalues move closer together, until the right eigenvalue (say λ_2) crosses the origin and enters stable territory, at $c = 1$. The fixed point is then a stable node, until $c = c_s = 0.8783...$ There, the eigenvalues meet on the negative real axis, only to immediately part again. The eigenvalues leave the real axis in opposite directions, tracing symmetric paths that bend towards the y-axis. The fixed point is then a stable spiral, up until the eigenvalues cross the y-axis. This happens at $c = 0.55$, and the fixed point is then locally surrounded by closed orbits. When c decreases further, the eigenvalues continue their heart-shaped paths in the right half plane, while the fixed point is an unstable spiral. The eigenvalues meet again on the positive real axis, when $c = c_u = 0.1259...$ The fixed point is then a repellor node, while the eigenvalues move in opposite directions on the real axis, towards their initial locations (left for λ_1, right for λ_2). At $c = a = 0.1$, λ_1 crosses into the left half plane, making the fixed point a saddle point. This continues until $c = 0$, when both eigenvalues arrive at the origin, and the fixed point disappears.

Between $0.446... < c < 0.55$, the phase portrait contains a limit cycle (the purple orbit in fig. 11). The parameter value where the limit cycle first appears is determined numerically to be $c_h = 0.44597197....$ For increasing c, the limit cycle tightens around the central fixed point, until it coalesces with it at $c = (1 + a)/2 = 0.55$. The fixed point is then an attracting spiral with a large basin of attraction. Going back in the other direction, for decreasing c, both the orbit period and the limit cycle become increasingly large. In the limit for $c = c_h$, the limit cycle coincides with the stable manifolds of the two neighbouring saddle points ($(a,\ 0)$ and $(1,\ 0)$), and the orbit period becomes infinite. At this bifurcation point $c = c_h$, the two saddle points on the x-axis are connected in a heteroclinic orbit. Analogously to the 'homoclinic bifurcation' from **Strogatz1994 Strogatz1994 Strogatz1994**, this bifurcation could be called a 'heteroclinic bifurcation'.

These differences in limit cycle behaviour can be observed in fig. 12. A near-harmonic oscillation yields regular, sine-like time series. Their amplitude is roughly the same as their initial amplitude (closed orbit-like behaviour). On the other hand, a near-heteroclinic cycle yields more exotic time series, with a longer period. The amplitude also grows quickly to the limit cycle amplitude, irrespective of the initial condition. Finally, each oscillation period contains a long interval where both time series are minimal and near constant. This happens when the trajectory comes close to the slow, stable manifold on the x-axis

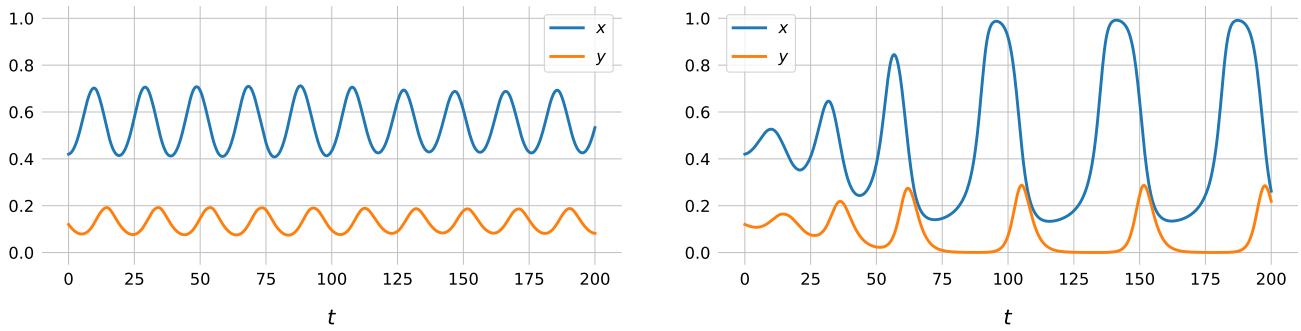

Figure 12: **Limit cycle simulations**. Simulated trajectories $x(t)$ and $y(t)$ for a near-harmonic oscillation (left, $c = 0.55$) and a near-heteroclinic orbit (right, $c = 0.46$). In both simulations, the initial phase point was $(0.42, 0.12)$.

3.2 Bifurcation analysis

A bifurcation diagram for $d = 0$ (fig. 13) confirms the previous stability analyses and phase space diagrams. Each of the four fixed points corresponds to a straight-line branch in the bifurcation diagram: at constant x for the first three fixed points, and increasing proportionally to c for the fourth, complex fixed point. At $c = 0.55$, we find indeed that this fourth fixed point switches from unstable to stable. At $c = 1$, it switches stability with the fixed point at $x = 1$ in a transcritical bifurcation.

Regarding periodic solutions: for a set of example values of c, the limit cycle and its period were calculated numerically (see e.g. fig. 11, middle row). This confirmed that the limit cycle amplitude is approximately linear in c, as drawn in fig. 13.

For $d \neq 0$, the transcritical bifurcation at $c = 1, x = 1$ disappears (fig. 14): for $d > 0$, the top-right and bottom-left branches in the (c, x)-plane join, while for $d < 0$, the bottom-right and top-left branches join. In the (c, y)-plane, the branches form a loop in the left-hand side of the plane for $d > 0$, and in the right-hand side of the plane for $d < 0$. (A similar phenomenon occurs at the fixed points-crossing for $c = a = 0.1$; although this is not a transcritical bifurcation, as both fixed points are unstable there).

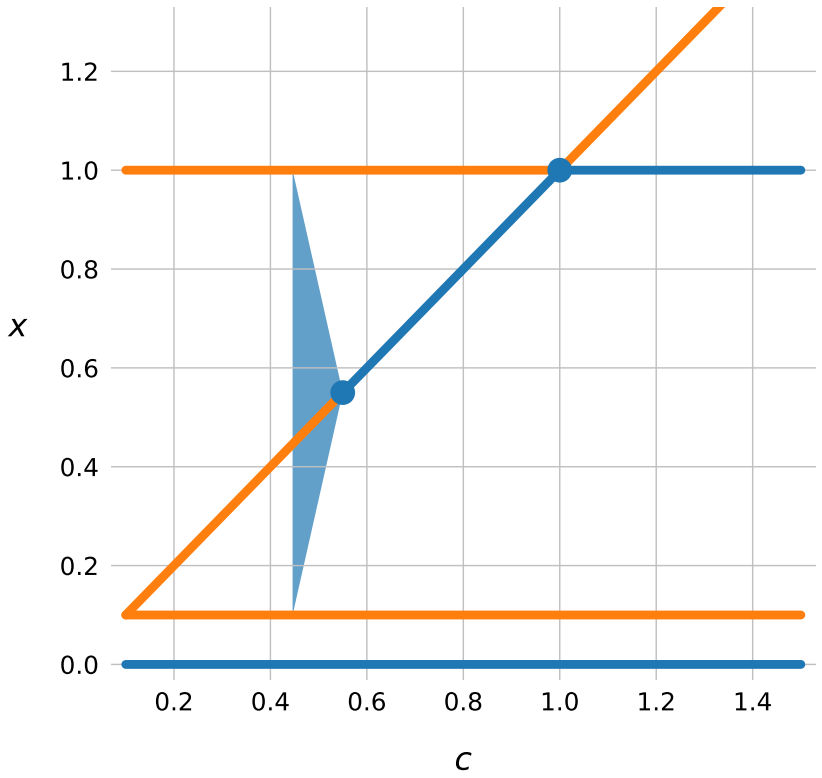

Figure 13: **Bifurcation diagram for $d = 0$.** (c, x)-plane projection. Orange lines represent unstable fixed points, while blue lines represent stable fixed points. The blue shaded region indicates the x-range of the limit cycle. Important bifurcations that are visible here are the heteroclinic cycle (and the start of the limit cycle) at $c = c_h = 0.446..$, the closed orbit behaviour at $c = 0.55$ (central blue circle), and the transcritical bifurcation at $c = 1$ (top right blue circle).

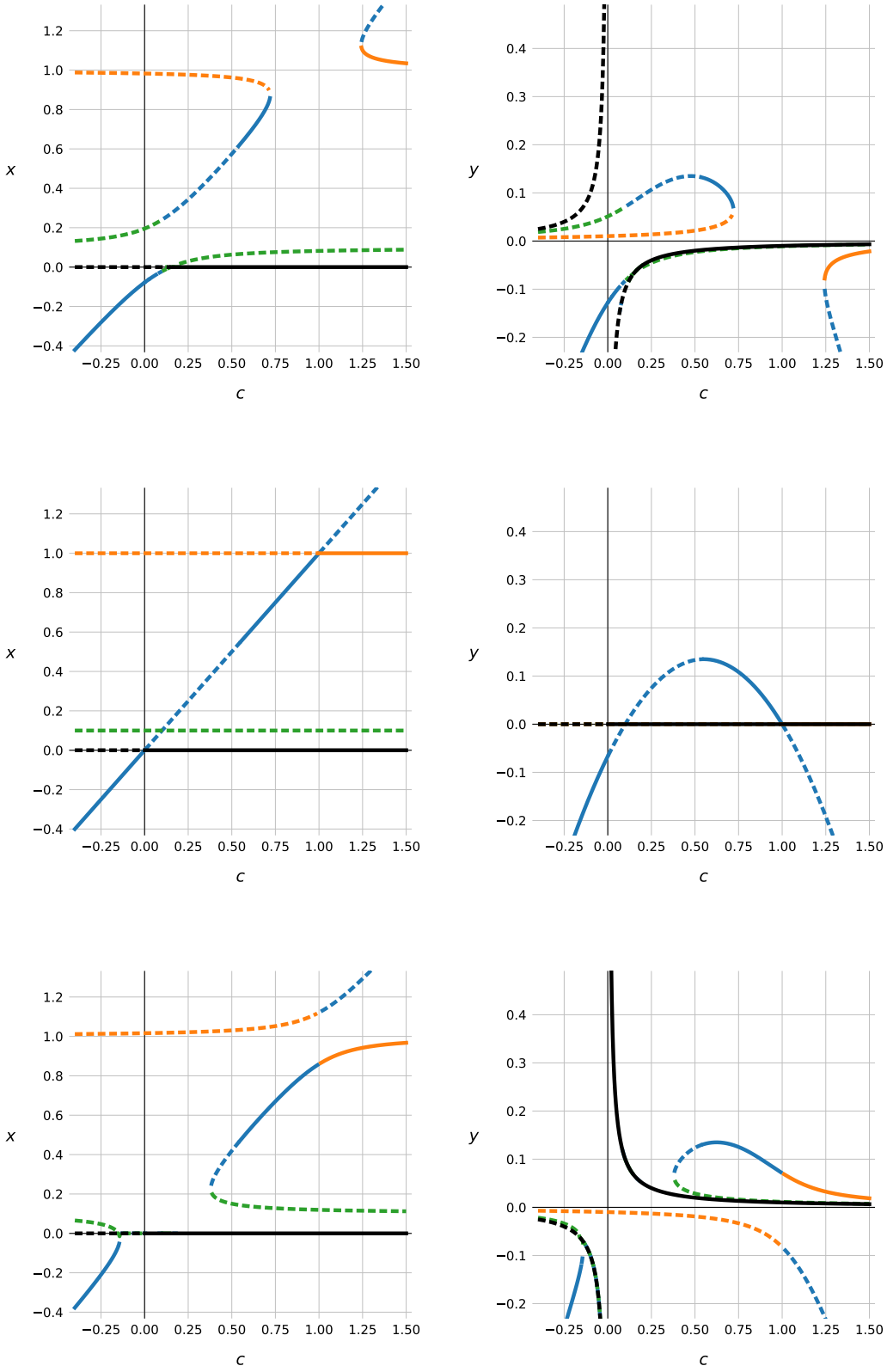

Figure 14: **Bifurcation diagrams**. *Top*: $d = 0.01$. *Middle*: $d = 0$. *Bottom*: $d = -0.01$. Dashed lines indicate unstable fixed points and solid lines indicate stable fixed points. Branches are coloured according to their corresponding fixed point (same colours as fig. 11; with the fixed point at $x = 0$ indicated in black here).

4 Aero-elastic galloping

From Newton's second law and introducing $x = \dot{y}$ as the linear velocity of the bridge element, its motion can be described by

$$\begin{aligned} \dot{x} &= 0.5\, V^2\, C(x/V)\ - x - 100y \\ \dot{y} &= x \end{aligned}$$

where the constants have been substituted in, and with $C(\alpha) \approx 10^{-2}\, \alpha - 10^{-3}\, \alpha^3 + 10^{-5}\, \alpha^5 - 10^{-8}\, \alpha^7$ (exact coefficients as in the assignment).

The system has a fixed point at the origin. Figure 15 shows the eigenvalues of the Jacobian at this fixed point, for varying wind speeds V. In low-wind conditions, the system starts out stable, with both eigenvalues having negative real parts (but having nonzero imaginary parts, predicting oscillatory behaviour). At $V = V_C = 42.5985...$, the eigenvalues cross the imaginary axis, and the origin transitions from a stable spiral, through a center, to an unstable spiral. V_C is the solution to $\tau = 0$, with $\tau = V\, A_1/2 - 1$ the trace of the Jacobian at the origin. For very large $V = V_R = 894.6..$, the eigenvalues land on the real axis, and the unstable spiral transitions to a repelling star and a repelling node. V_R is the solution to $4\Delta = \tau^2$, with $\Delta = 100$ the determinant of the Jacobian at the origin (see chapter 3). Table 2 summarises this classification of the origin's stability.

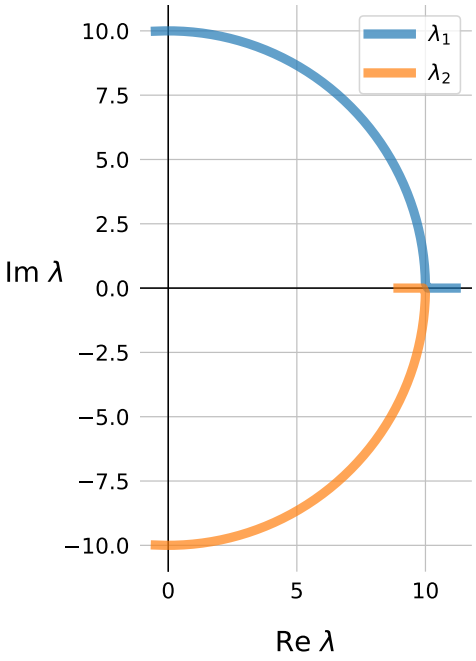

Figure 15: **Linear stability analysis of the bridge model**. Eigenvalues of the Jacobian at the fixed point $(0, 0)$, for $V \in [0, 900]$ ($V = 0$ in the left half plane, at Re $\lambda_i = -0.5$).

Wind speed V	Stability of origin
$V < V_C$	Stable spiral
$V = V_C$	Center
$V_C < V < V_R$	Unstable spiral
$V = V_R$	Repelling star
$V > V_R$	Repelling node

Table 2: **Classification of the fixed point**. $V_C = 42.6..$ and $V_R = 894.6..$

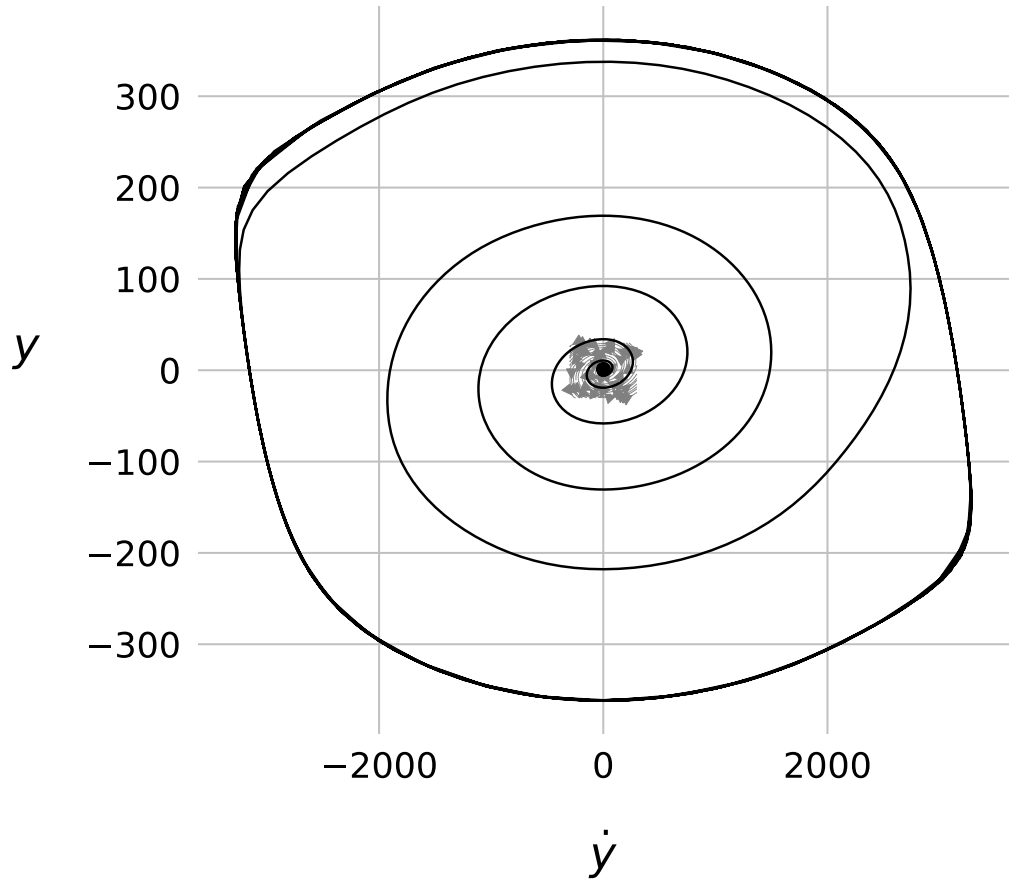

Figure 16: **Phase space diagram of the bridge model**. Here for $V = 300$.

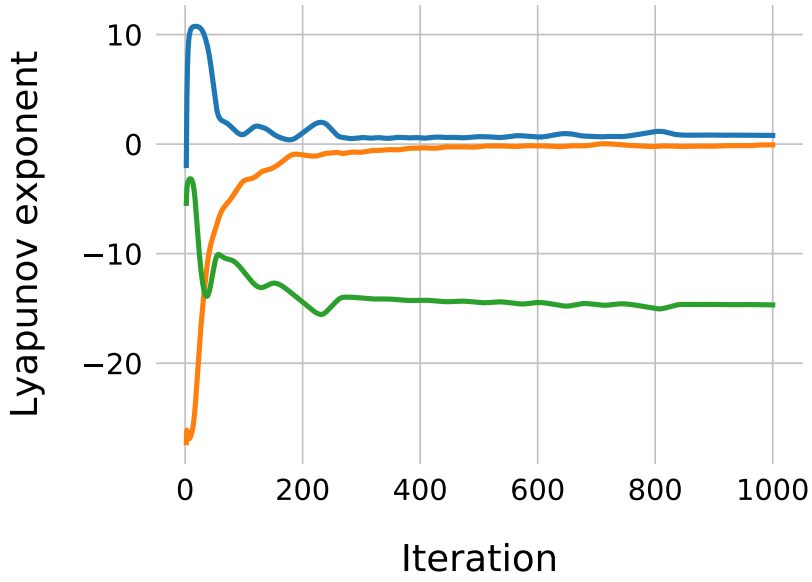

Figure 17: **Estimating Lyapunov exponents of the Lorenz system**. Initial phase point $(1, 1, 1)$. Final exponent estimates are $0.79, -0.07$, and -14.7.

5 Chaos

5.1 Lyapunov exponents of the Lorenz equations

The algorithm integrates both an initial phase point and the spatial gradient of the phase point along the trajectory over fixed time steps `st` (via the simplest first order Euler method). Next, an orthogonal basis is sought for the new spatial gradient, via the Gram-Schmidt algorithm. The cumulative sum of logarithms of the Gram-Schmidt scaling factors divided by the total time elapsed is then the estimate of the Lyapunov exponent. This is integration-orthogonalisation loop is repeated for a given number of iterations `kkmax`.

When the time step is too large (e.g. `st = 0.1` here), the exponents diverge. When it is too small on the other hand (`st = 0.001` here), the convergence is extremely slow. Even for a balanced time step (like `st = 0.01` here), enough iterations need to be taken yield a decent result (e.g. `kkmax > 400` here; see fig. 17). The initial phase point also influences the results. A different phase point as in fig. 17 ($(6, 6, 6)$) yields better estimates for example ($0.89, -0.04$, and -14).

Interestingly, using a more advanced ODE solver (like a higher order Runge-Kutta method) or orthogonalisation algorithm (like a singular value decompostion via the QR-algorithm) yields markably worse results.

5.2 Hindmarsh-Rose neuron model

The system behaves chaotically in random burst mode (fig. 18, top): even the tiniest perturbation to the initial phase point renders $x(t)$eventually unpredictable. The burst generation mode is not chaotic: even relatively large perturbations do not qualitatively change the phase space trajectories (fig. 18, bottom).

5.3 Chua's circuit

A simulation of the Chua circuit displays chaotic behaviour (fig. 19). Estimating the Lyapunov exponents according to the method of section 5.1 confirms this: the largest exponent $\approx 0.16 > 0$ (fig. 20).

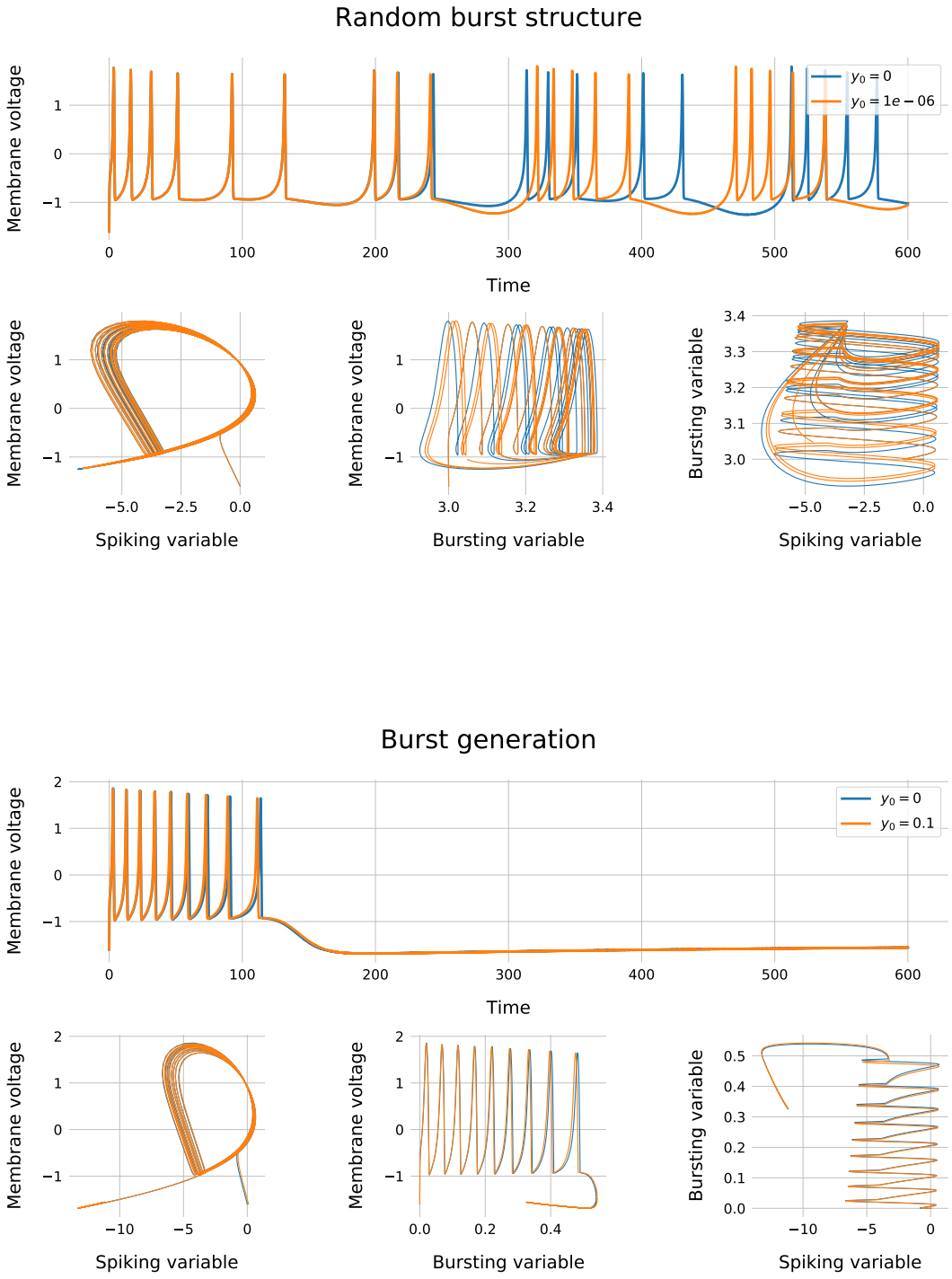

Figure 18: **Hindmarsh-Rose neuron model**. See text for interpretation. (In random burst mode, the initial slow current was $z(0) = 3$, while in burst generation mode, it was $z(0) = 0$. Other parameters as instructed).

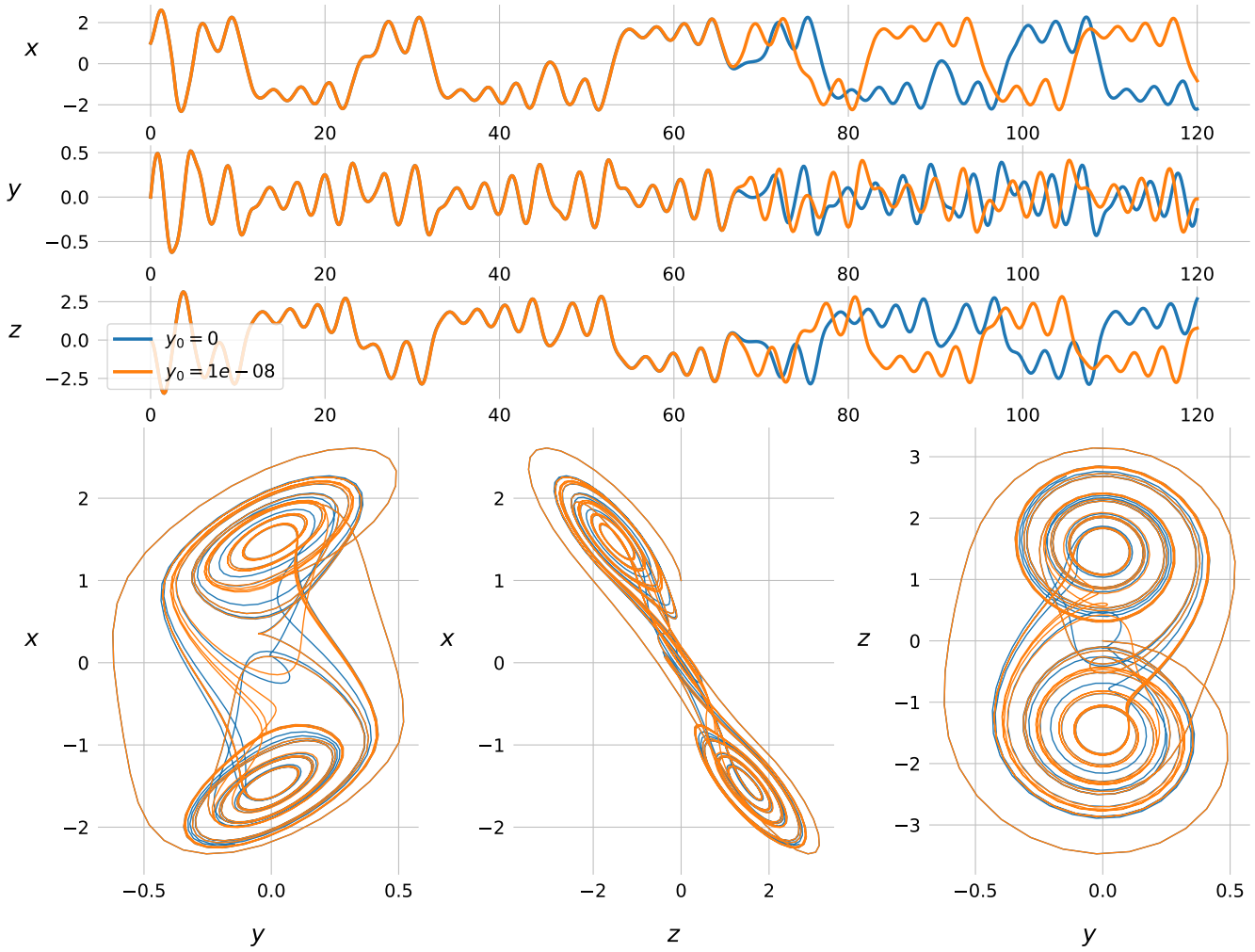

Figure 19: **Chua circuit model**. Time series (top) and phase space projections (bottom). Note the chaotic behaviour and the double-scroll dynamics. (Initial condition $(1, y_0, 0)$, with y_0 as indicated).

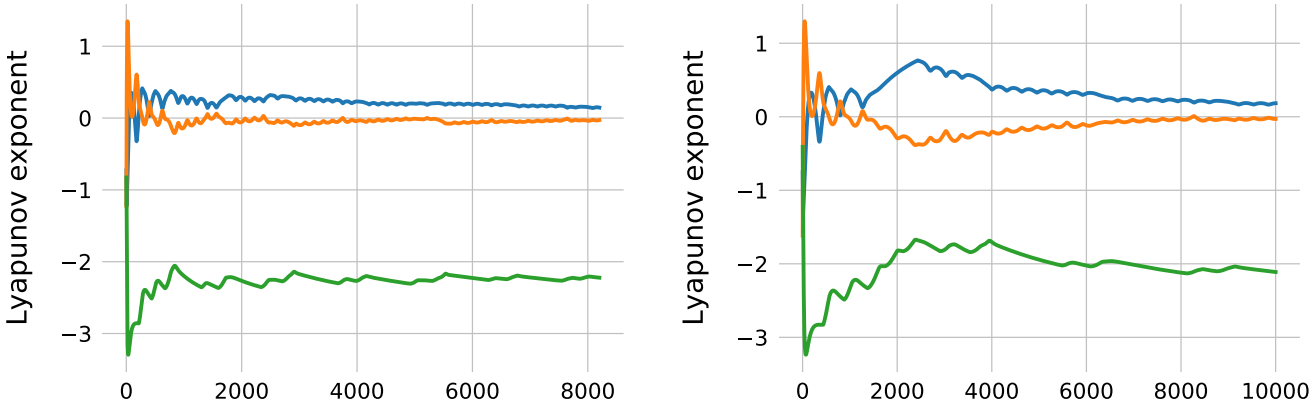

Figure 20: **Estimating Lyapunov exponents of the Chua circuit**. *Left*: `st = 0.01`, final largest exponent 0.146. *Right*: `st = 0.005`, final largest exponent 0.184.